Rolapitant is a reversible inhibitor of CYP2D6

Sarah M. Glass, Sabrina M. Leddy, Michael C. Orwin,

Garrett Miller, Kyle A. Furge and Laura Lowe Furge

Department of Chemistry, Kalamazoo College, Kalamazoo, MI, USA

Running Title: Rolpitant interactions with CYP2D6

Corresponding Author: Laura Lowe Furge, Department of Chemistry, Kalamazoo College, 1200 Academy Street, Kalamazoo, MI 49006. Tel: 269-337-7020; Fax: 269-337-7251. Email: Laura.Furge@kzoo.edu.

Number of Text Pages: 31

Number of Tables: 0

Number of Figures: 7

Number of References: 34

Number of words in Abstract: 243

Number of words in Introduction: 303

Number of words in Discussion: 735

Abbreviations used: CYP, cytochrome P450 enzyme; HLM, human liver microsomes; HPLC, high performance liquid chromatography; PRL, protonated +1 rolapitant.

DMD Fast Forward. Published on April 5, 2019 as DOI: 10.1124/dmd.118.085928
This article has not been copyedited and formatted. The final version may differ from this version.

Abstract

Rolapitant (Varubi®) is a high affinity NK1 receptor antagonist that was approved in September 2015 as a treatment for nausea and vomiting caused by chemotherapy. *In vivo* rolapitant moderately inhibits CYP2D6 for at least seven days after one 180 mg dose. Due to the long inhibition time, we investigated rolapitant as a possible mechanism-based inactivator of CYP2D6. Rolapitant docked in the active site of CYP2D6 and displayed type I binding to CYP2D6 with K_s of 1.2 ± 0.4 μM. However, in NADPH-, time-, and concentration-dependent assays of CYP2D6 activity, no evidence for mechanism-based inactivation and no metabolites of rolapitant were observed. Stopped-flow binding studies yielded k_{on}/k_{off} (K_d) of 6.2 μM. The IC_{50} for rolapitant inhibition of CYP2D6 activity was 24 μM suggesting that inhibition is not due to tight-binding of rolapitant to CYP2D6. By Lineweaver-Burk analysis, rolapitant behaved as a mixed, reversible inhibitor. K_i values of 20 μM and 34 μM were determined by Dixon analysis, with bufuralol and dextromethorphan as reporter substrates, respectively, and drug-drug interaction modeling did not predict the reported *in vivo* inhibition. The interaction of rolapitant with CYP2D6 was also examined in 1 μsec molecular dynamics simulations. Rolapitant adopted multiple low energy binding conformations near the active site, but at distances not consistent with metabolism. Given these findings, we do not see evidence that rolapitant is a mechanism based inactivator. Moreover, the reversible inhibition of CYP2D6 by rolapitant may not fully account for the moderate inhibition described *in vivo*.

Introduction

Rolapitant is a high affinity NK1 receptor antagonist recently approved under the name Varubi® as a treatment for nausea and vomiting caused by chemotherapy by the U.S. Food and Drug Administration (Figure 1) (FDA, 2015; Tesaro, 2015). Rolapitant is metabolized *in vivo* primarily by CYP3A4 to form the major metabolite M19 (C4-pyrrolidine-hydroxylated rolapitant) (FDA, 2015). However, in animal studies the majority of the drug is excreted unmetabolized (~14% in urine and ~73% in feces over 6 weeks) (Tesaro, 2015).

One advantage of rolapitant over other available antiemetics is that it does not inhibit or induce CYP3A4 (Poma et al., 2013; FDA, 2015) – the CYP most involved in the metabolism of pharmaceutical drugs (Guengerich, 2015). Given the lack of CYP3A4 inhibition, rolapitant is believed to reduce drug-drug interactions (Olver, 2015). However, rolapitant has been shown to moderately inhibit the activity of CYP2D6 for at least seven days after only one 180 mg dose (FDA, 2015; Wang et al., 2018).

Due to the long inhibition time and increased AUC (~3-fold higher with dextromethorphan as victim drug) (Tesaro, 2015) in clinical studies, rolapitant was investigated as a possible substrate and mechanism-based inactivator of CYP2D6. Rolapitant has a basic nitrogen and aromatic rings with a molecular weight of 500.5 g/mol (Figure 1). Of the over ninety substrates in the CYP2D6 Small Molecule Kinetics Database, only two substrates for CYP2D6 [e.g. amiodarone (645.3 g/mol) and ritonavir (720.9 g/mol)] have molecular weights larger than that of rolapitant (Chico et al., 2009).

Our initial studies showed that rolapitant could dock in the active site of CYP2D6 in an orientation consistent with metabolism. Furthermore, spectral binding titrations

produced Type 1 binding, consistent with binding of a substrate (*vide infra*). The goal of the present study was to examine the mechanism by which rolapitant achieves long term inhibition of CYP2D6 *in vivo*.

DMD Fast Forward. Published on April 5, 2019 as DOI: 10.1124/dmd.118.085928
This article has not been copyedited and formatted. The final version may differ from this version.

Materials and Methods

Chemicals. Rolapitant was purchased from AdooQ Bioscience (Irvine, CA) and reconstituted in DMSO for use in assays described below. Ultra-pure solvents (water, ACN, and methanol) for MS were purchased from EMD Chemicals, Inc. (Gibbstown, NJ). All other solvents were HPLC grade and purchased from Sigma-Aldrich (St. Louis, MO). Bufuralol (mixture of enantiomers) and hydroxyl-bufuralol were from Toronto Research Chemical (North York, Ontario, Canada). Potassium phosphate, NADPH, dextromethorphan, dextrorphan, and all other reagents were purchased from Sigma-Aldrich (St. Louis, MO).

Enzymes. Supersomes™ (Corning Life Sciences, Tewksbury, MA) were used in all assays except spectral binding titrations and stopped-flow spectroscopy. For spectral binding titrations and stopped-flow spectroscopy, purified CYP2D6 and CYP3A4 were used; expression and purification were as described elsewhere (Gillam et al., 1993; Gillam et al., 1995; Hanna et al., 2001; Glass et al., 2018).

Time Dependent Inactivation of CYP2D6 Supersomes™ with rolapitant. Four primary reaction mixtures of CYP2D6 Supersomes™ (20 pmol) in potassium phosphate buffer (pH 7.4, 100 mM) were incubated in a 37°C shaking bath for 3 minutes. Two of these mixtures contained rolapitant (5 μM) and two contained DMSO for solvent vehicle control. After 3 minutes, two primary reaction mixtures (one with and one without rolapitant) were initiated with NADPH (1 mM). The other two received water as a control. The final reaction volume was 100 µL. Aliquots (10 μL) of the primary reaction were removed at various time points (0, 1, 5, 10, 15, 30 minutes) and transferred to a secondary reaction containing bufuralol (100 μM), NADPH (1 mM), and potassium

phosphate buffer (pH 7.4, 100 mM). The final secondary reaction volume was 200 μL. Reactions were quenched with 30 μL ACN after 10.5 minutes. Samples were then centrifuged (16,100 x g) for five minutes and 10 μL of the supernatant were injected onto a Waters Symmetry C18 column (5 µm, 3.9 x 150 mm, Waters Corporation, Milford, MA) connected to a Waters e2965 HPLC (Milford, MA) paired with a Waters 2475 fluorescence detector (Milford, MA). The instrument method and mobile phase were the same as previously described with bufuralol (Nagy et al., 2011; Glass et al., 2018). The 1'-OH-bufuralol peak area was converted to concentration using a standard curve.

Concentration Dependent Inactivation CYP2D6 Supersomes™ with rolapitant. Ten primary reaction mixtures of 2D6 Supersomes™ (20 pmol), potassium phosphate buffer (pH 7.4, 100 mM), and varying concentrations of rolapitant (0-40 μM) and were incubated in a 37°C shaking bath for 3 minutes, as indicated in figure legends. The 0 μM rolapitant reaction contained DMSO as a control. After 3 minutes, five of the reactions (one for each concentration of rolapitant) were initiated with NADPH (1 mM), while the other five received water as a control. The final reaction volume was 50 μL. Aliquots (10 μL) of the primary reaction were removed 20 minutes after initiation and transferred to secondary reaction mixtures containing NADPH (1 mM), bufuralol (100 μM), and potassium phosphate buffer (pH 7.4, 100 mM). The final secondary reaction volume was 200 μL. Reactions were quenched with 30 μL of cold ACN after 10 minutes. Samples were then centrifuged (16,100 x g) for five minutes and 10 μL of the supernatant was analyzed as described above.

Rolapitant Metabolites formed by 2D6 and 3A4 Supersomes™. Rolapitant (50 μM) in potassium phosphate buffer (pH 7.4, 100 mM) was combined with either

CYP2D6 or CYP3A4 Supersomes™ (20 pmol). The mixtures were pre-incubated for 3 minutes at 30 °C in a shaking bath before initiation by NADPH (1 mM). The final reaction volume was 100 μL. The reactions proceeded for 30 minutes before being quenched with 20 μL ACN and placed on ice. The samples were centrifuged (16,100 x g) for 5 minutes and 10 μL of the supernatant were injected onto a Kinetex C18 column (2.6 µm, 100 Å, 100 x 2.10 mm; Phenomenex, Torrance, CA) connected to a Waters Alliance 2690 HPLC system (Milford, MA). A gradient separation system was achieved using 0.1% formic acid in MS grade water (Solvent A) and 0.1% formic acid in acetonitrile (Solvent B). The initial conditions were 90% A and 10% B. These conditions were held for five minutes. At 30 minutes, the conditions were 10% A and 90% B. These conditions were held for five minutes. At 40 minutes, the gradient returned to initial conditions, which were held for an additional ten minutes. The total run time was 50 minutes, with a flow rate of 0.1 mL/min. The samples were analyzed using a Thermo-Fisher Scientific LXQ MS in the positive ion mode (Waltham, MA).

Binding Studies. Spectral binding titrations for determination of K_s were performed as previously described (Nagy et al., 2011). Briefly, purified CYP2D6 (1 μM) or CYP3A4 (2 μM) in potassium phosphate buffer (pH 7.4, 100 mM) was divided evenly between two micro quartz cuvettes. A baseline was taken from 350-500 nm with a Cary 300 spectrophotometer (Agilent, Santa Clara, CA). Rolapitant (0.05-150 μM, final) was then added to the sample cuvette while an equal volume of DMSO added to the reference cuvette. Spectra from 350-500 nm were recorded after each addition. The total amount of DMSO added did not exceed 2% (v/v) DMSO. Titrations with both CYP2D6 and CYP3A4 were Type I. Differences in absorbance between 390 nm and 420 nm were

plotted against concentrations of ligand and fit with the quadratic velocity equation, or tight-binding equation: $[CYP\bullet rolapitant] = 0.5(K_s + E_t + S_t) - [0.25(K_s + E_t + S_t)^2 - E_tS_t]^{1/2}$ where S represents substrate concentration, E is the total enzyme concentration, and K_s is the spectral dissociation constant for the reaction CYP + rolapitant $\rightleftharpoons$ CYP•rolapitant. The dissociation constant, K_s, was determined using KaleidaGraph software (Synergy Software, Reading, PA). Spectra for each concentration were adjusted so each scan intersected at 0 absorbance at the isobestic point (407 nm).

Stopped-flow spectroscopy was used to determine k_{on} and k_{off} using a rapid scanning monochrometer OLIS RSM-1000 stopped flow instrument (On-Line Instrument Systems) in the laboratory of Dr. F. P. Guengerich (Vanderbilt University). Stopped-flow sample syringes contained 50 mM potassium phosphate buffer (pH 7.4) and either 4 μM purified CYP2D6 or rolapitant (2-100 μM) diluted in water. Equal volumes from both syringes were injected in the sample cell (4 x 20-mm) at room temperature with a final volume of 2 mL. Absorbance spectra from 350-500 nm were recorded at one millisecond intervals for a total of 4 seconds. Data were not collected during the initial 4 ms mix time. Data subsets at the absorbance maxima and minima (390 and 420 nm, respectively) were created on the OLIS software for each rolapitant concentration and then subtracted to create the composite absorbance changes over time ($\Delta A_{390\text{-}420}$). At least three replicates of each ligand concentration were averaged and plotted over time. Experiment parameters ([E] and [L], enzyme and ligand, respectively) were entered and the data was fit to a minimal kinetic model (single step second order reaction, E + L → EL) to estimate binding constants using KinTek Global Kinetic Explorer software (KinTek, Snow Shoe,

PA). The K_d value for rolapitant dissociation from CYP2D6 was calculated from k_{off}/k_{on}. Rolapitant residence time (t_R) was calculated as $1/k_{off}$.

Determination of K_i for rolapitant with CYP2D6 Supersomes™. Reaction mixtures contained rolapitant (0-100 μM), bufuralol (5-100 μM) or dextromethorphan (5-100 μM), CYP2D6 Supersomes™ (2 pmol), and potassium phosphate buffer (pH 7.4, 100 mM), as indicated in figure legends. The reaction mixture was incubated in a 37 °C shaking bath for 3 minutes and then initiated with NADPH (1 mM). The final reaction volume was 100 μL. Reactions were quenched with 20 μL ACN and placed on ice after a time determined to be in the linear range for product formation. Samples were then centrifuged (16,100 x g) for 5 minutes and 10 μL of the supernatant were analyzed as previously described (Glass et al., 2018). Lineweaver-Burk and Dixon plots were created using KaleidaGraph (Synergy Software, Reading, PA). All experiments were run in quadruplicate.

Determination of IC_{50}. CYP2D6 Supersomes™ (2 pmol) were incubated with dextromethorphan (10 μM) and quinidine (0-50 μM) or rolapitant (0-100 μM) in potassium phosphate buffer, pH 7.4 (100 mM). Quinidine was dissolved in methanol and rolapitant in DMSO. Incubations contained no more than 2% organic (v/v). The final reaction volume was 100 μL. Reactions were incubated in a 37 °C shaking bath for 3 minutes before being initiated with NADPH (1 mM). Reactions were quenched with 20 μL of cold ACN after 10 minutes. Samples were then centrifuged (16,100 × g) for five minutes and dextrorphan product formation was measured as previously described (Glass et al., 2018).

Molecular Dynamics with Rolapitant. Simulation setup and initialization was performed largely as described previously (de Waal et al., 2014). Briefly, for system setup a 2.8 Å crystal structure of CYP2D6 bound to prinomastat (PDB ID:3QM4, Chain A) was used for starting protein and heme coordinates with the exception that the prinomastat ligand was removed. The AMBER99SB and GAFF force field were used for protein and heme model parameters along with quantum mechanically derived parameters for the oxygen complex in a resting high spin Compound I state (Shahrokh et al., 2012). The protein+heme+oxygen system was solvated in a 10 Å pad of TIP3P waters and neutralized. RESP charges for protonated rolapitant (+1) (PRL) were derived using the Gaussian09_E.01 option from R.E.D. Server (Vanquelef et al., 2011). AutoDock Vina (http://autodock.scripps.edu) (Morris et al., 1998; Huey et al., 2007; Trott and Olson, 2010) was used to identify an initial pose of PRL near the CYP2D6 heme to produce a combined protein+heme+oxygen+ligand system. The initial pose of rolapitant was chosen by visual inspection of the lowest energy poses.

Following system setup, the system was solvent energy minimized, full system energy minimized, heated, NPT and NVT pressurized as previously described (de Waal et al., 2014) using pmemd.cuda (Amber16). One microsecond (1 μsec) MD simulations were performed using a version of pmemd.cuda that was modified to incorporate an adaptive biasing potential as described by Dickson *et al*. (Dickson et al., 2016). While the initial adaptive biasing potential implementation was integrated with GROMACS (Dickson et al., 2016), our version was modified for use with Amber16 and generously provided to us by Parker de Waal (Van Andel Research Institute, Grand Rapids, MI). In these types of simulations, a very small amount of energy is deposited at

the space where the ligand currently occupies. Accumulation of small energy 'hills' during the simulation encourages the ligand to move and therefore sample more configuration space during a given simulation run. Without the use of biasing strategies (e.g. filling in low energy wells), the likelihood of the ligand moving significantly within the active site or egressing during a 1 μsec simulation is extremely small. In addition, tracking where energy is deposited can be used to estimate rolapitant's low-energy binding positions. A schematic of our approach to adaptive biasing simulations is shown in Supplemental Figure 1. To prevent ligand diffusion, a spherical ligand restraint was included such that the sphere was at least 6 Å from any CYP2D6 atom (Supplemental Figure 1-A,B). Biasing parameters were set at c = 0.01 and b = 0.8. The simulation was run for 5 x 10^8 steps with each step representing 2 femtoseconds. Each simulation took approximately 10 days to complete on a NVIDIA GeForce GTX 980 Ti GPU.

Tracking the position of every rolapitant atom during the adaptive biasing simulation run is computationally complex. To reduce this computational complexity, adaptive biasing schemes track a courser grained representation of the ligand by "collecting" different parts of the ligand into a single variable In our models, the root mean square deviation (RMSD) of two collections of atoms, "Protonated Rolapitant Collective Variable 1" (PRL-CV1) and "Protonated Rolapitant Collective Variable 2" (PRL-CV2) are tracked by the adaptive biasing algorithm versus a reference point near the heme (Supplemental Figure 1-C,D,E). These CV atoms were picked so that the biasing potential did not track redundant or superfluous motion, but did track overall rolapitant movement. The reference point near the heme was picked to identify

alternative low energy binding poses with higher resolution. Additionally, monitoring the accumulation of the energy deposition that is required to get the ligand to move from a particular location can be used to estimate the free energy at that location (Supplemental Figure 1-F,G).

Free energy binding landscapes produced from the adaptive biasing simulations were visualized using the R 3.2.3 statistical framework (Team, 2017) with the "lattice" library version 0.20.23 (Sarkar, 2008). Rolapitant egress trajectories and molecular images were produced using Visual Molecular Dynamics, VMD, 1.9.3 (University of Illinois, Urbana-Champaign).

Results

In spectral binding titrations, rolapitant displayed type I spectral binding with respect to binding both CYP2D6 and CYP3A4 as observed by an increase in absorbance at 390 nm and a decrease at 420 nm (Figure 2). Spectral binding affinity (K_s) was calculated to be 1.2 ± 0.4 μM for CYP2D6 and 16 ± 2 μM for CYP3A4 indicating much tighter binding to CYP2D6 (Figure 2).

Based on this observation we hypothesized that perhaps inhibition of CYP2D6 *in vivo* might be due to a slow off-rate for rolapitant from CYP2D6. Stopped-flow measurement of k_{on} and k_{off} rates for rolapitant from CYP2D6 yielded a k_{on} of 1.12 x 10^6 $M^{-1}s^{-1}$ and a k_{off} of 7.04 s^{-1} using a global exponential fit (Figure 3) A k_{off} of 7.04 s^{-1} indicates a residence time (t_R) of rolapitant with CYP2D6 of 0.142 seconds. The K_d value for rolapitant with CYP2D6, calculated from k_{off}/k_{on}, was 6.2 μM and was similar to the observed K_s.

Time- and concentration-dependent inactivation assays showed that rolapitant did not behave as a mechanism-based inactivator of CYP2D6 (Supplemental Figure 2). Also, no metabolites of rolapitant reactions with CYP2D6 were observed (data not shown). To test possible inactivation of CYP2D6 by metabolites of CYP3A4 or other drug-metabolizing enzymes, co-incubation assays containing either mixed CYP3A4 with CYP2D6 Supersomes™ or human liver microsomes mixed with CYP2D6 Supersomes™ were completed (data not shown). Over time, no inactivation of CYP2D6 was observed in these conditions suggesting that rolapitant is not metabolized to another form that could serve to inactivate CYP2D6.

A further possibility was that rolapitant could be a tight-binding reversible inhibitor of CYP2D6. The drug quinidine is a classic example of a tight-binding inhibitor of CYP2D6 that strongly inhibits the activity of CYP2D6, but does not have a long *in vivo* half-life (6-8 hours elimination half-life) (Zhou, 2009). In IC_{50} assays, quinidine showed a biologically relevant IC_{50} value of 0.06 μM (e.g. 60 nM) similar to values previously reported (Hutzler et al., 2003) (Supplemental Figure 3). In comparison, the IC_{50} for rolapitant was three orders of magnitude higher at 24 μM (Figure 4).

Given that reversible inhibition was observed, Lineweaver-Burk analysis and Dixon analysis were competed to determine the type and extent of inhibition. From Lineweaver-Burk analysis with two different substrates (dextromethorphan and bufuralol), mixed inhibition was observed (Figure 5). Both the K_m and v_{max}, for either dextromethorphan or bufuralol metabolism, were altered with increasing concentrations of rolapitant in the reactions. K_m values increased roughly 2-3-fold while v_{max} was approximately halved . Plotting of the kinetic data in Michaelis-Menten style plots did not reveal any reporter substrate inhibition of CYP2D6 over the range of substrate concentrations used in our analysis (data not shown). Dixon analysis yielded K_i values of 20 μM and 34 μM with bufuralol and dextromethorphan as reporter substrates, respectively (Figure 6).

Using the K_i values from Dixon analysis, static drug-drug interactions were modeled using the 2017 FDA DDI guidance for industry predicted ratio (R1) calculation of $1 + ([I]_{max,u}/K_i)$ (FDA, 2017) where R1 is the predicted ratio of the victim drug's AUC in the presence and absence of rolapitant, $[I]_{max,u}$ is the concentration of rolapitant unbound, and K_i is the inhibition constant. *In vivo*, after a single 180 mg dose, the C_{max} of

rolapitant has been reported to be ~ 2.5 μM and rolapitant is ~99% bound in the plasma (Wang et al., 2017). For DDI calculations, only unbound drug concentration as used. From this, the R1 value for rolapitant was ~1.0. This value, according to FDA guidance, does not predict DDI with CYP2D6. We note that using DDI calculation standards prior to 2017, e.g. at the time rolapitant was originally evaluated by the FDA, DDI modeling calculations used total drug concentration at C_{max} (~2.5 μM for rolapitant) and slight DDI were predicted. For comparison to rolapitant, we did the same R1 calculations with the IC_{50} data we generated with quinidine and literature values for quindine C_{max}. In the case of quinidine, R1 values of over 7 were calculated, consistent with strong inhibition as observed *in vivo*.

To better understand interactions of rolapitant with CYP2D6, ten-1 μsec molecular dynamics simulations were performed using approximately 100 days of GPU compute time. For rolapitant and CYP2D6, the residence time was 0.142 sec, or 1.42 x 10^5 μsec based on the k_{off} measured in stopped-flow experiments above. To compensate for disparity between the residence time (1.42 x 10^5 μsec) and our simulation times (1 μsec), we examined ligand binding and egress using molecular dynamics simulations modified to include an adaptive biasing potential as described in the Methods.

Rolapitant remained fully enclosed in the active site in six (6) simulations and moved outside of the protein in four (4) simulations (Supplemental Figure 4 and Supplemental Movie) via channels defined by the nomenclature of Wade (Cojocaru et al., 2007). In our 1 μsec simulations, rolapitant never re-entered the enzyme after egressing. Most commonly, protonated rolapitant bound in a fully extended pose in a pocket that was within 5 Å of mostly hydrophobic residues. There were some indications of pi-pi

interactions between rolapitant and Phe247 and Phe112, but the conformations for interactions were not consistent or strong (e.g. no pi-pi stacking) (Supplemental Figure 4, 5 and data not shown). Movement of Phe483 allowed access of rolapitant to the solvent channel (data not shown). Overall both the low energy binding poses and egress through the 2c channel are consistent with rolapitant behaving as a reversible inhibitor. We also noted that in all simulations, rolapitant was completely above the active site and outside of the range of metabolism.

DMD Fast Forward. Published on April 5, 2019 as DOI: 10.1124/dmd.118.085928
This article has not been copyedited and formatted. The final version may differ from this version.

Discussion

In vivo, rolapitant inhibits the activity of CYP2D6 for at least seven days following a single dose. Rolapitant is one of the largest ligands known to bind CYP2D6 and its mechanism of multi-day *in vivo* inhibition is unknown. In this study we examined several possible mechanisms for inhibition, including possible inactivation.

The spectral binding constant for rolapitant with CYP2D6 (1.2 ± 0.4 μM) was in a similar range as seen with other CYP2D6 ligands including several mechanism-based inactivators previously reported (~0.4 – 30 μM) (Nagy et al., 2011; Livezey et al., 2014). The low value for the spectral binding constant could lead to observed inhibition if the concentration of rolapitant were high enough *in vivo*. A single 180 mg dose of rolapitant produces a C_{max} value of ~2.4 µM *in vivo* (Wang et al., 2017). However, the IC_{50} and K_i values for rolapitant (24 μM for IC_{50} and 20 μM and 34 μM for K_i depending on substrate reporter) are greater than C_{max} *in vivo* concentrations of rolapitant. The K_i values for rolapitant are also similar to those reported for inhibition of CYP2D6 by amiodarone - a ligand inhibitor larger than rolapitant, and metoprolol - a smaller ligand inhibitor [26.8 μM and 11.8 μM for amiodarone and 17.0 μM and 11.3 μM for metoprolol with bufuralol and dextromethorphan as reporter substrates, respectively (VandenBrink et al., 2012)]. There was no observed metabolism of rolapitant by CYP2D6 and no time- or concentration-dependent inactivation (Supplemental Figure 2 and data not shown). CYP2D6 was also not inhibited in assays that included CYP3A4 and rolapitant (data not shown). Though the concentrations of M19 in the assays would be low, the lack of inhibition was consistent with a recent *in vivo* clinical study with rolapitant that suggested

that the M19 formed by CYP3A4 would not be a strong inhibitor of CYP2D6 (Wang et al., 2018).

The k_{on} and k_{off} values calculated from stopped-flow (1.12×10^6 $M^{-1}s^{-1}$ and 7.04 s^{-1}, respectively) were similar to those reported by Yun et al. for 7-OH coumarin binding to CYP2A6 (k_{on} of 2.0×10^6 $M^{-1}s^{-1}$, k_{off} of 6.8 s^{-1}, k_{off}/k_{on} = 3.4 μM; t_R = 0.147 seconds) (Yun et al., 2005) and overall did not suggest unusual individual rate constants as an explanation for inhibition.

In order to understand possible binding modes that might lead to inhibition, adaptive biasing molecular dynamics simulations were completed. In our simulations, both Asp301 and Glu216 acted as binding residues for rolapitant, but with the ligand was outside of metabolism range of the heme consistent with a lack of metabolism in *in vitro* studies. We also observed that Phe483 could play a role in directionality of ligand egress, particularly relevant to the solvent channel, as suggested in crystal structures of Wang et al. (Wang et al., 2015).

The hydrophobic binding area in our simulations is the same as those described in the crystal structures of CYP2D6 including both Rowland et al. and Wang et al. and in docking studies with CYP2D6 inhibitors and substrates by VandenBrink et al. (Rowland et al., 2006; VandenBrink et al., 2012; Wang et al., 2012; Wang et al., 2015). VandenBrink *et al*. further suggest that interactions in this binding pocket may influence inhibition. Similarly, in polymorphic forms of CYP2C9, Maekawa et al. found three different ligand binding sites – a peripheral site, an active site, and an access channel site and suggested that the access channel site might be a site for regulation of allosteric inhibition (Maekawa et al., 2017). Siu et al. recently described an allosteric binding

antechamber that was consistent with stabilization of CYP2D6 inhibition by celecoxib (Siu et al., 2018). Our findings, along with other previous findings, support the hypothesis that similar binding sites may be present in CYP2D6 as well and that binding in these sites may serve an inhibitory function.

Overall the molecular dynamics studies support plasticity in CYPs and support a model that ligands, particularly large ones, egress from CYP2D6, via multiple small-scale fluctuations rather than large swings or rotations. This is consistent with the suggestion by Rowland et al. in the first crystal structure of CYP2D6 that such fluctuations would be normal and necessary for ligand movement within protein channels (Rowland et al., 2006). In addition, since rolapitant was not a mechanism-based inactivator or a tight-binding inhibitor of CYP2D6, the observed *in vivo* inhibition of CYP2D6 by rolapitant may be simply due the long 7 day *in vivo* half-life.

Acknowledgement. We thank Parker de Waal and Dr. Brad Dickson for helpful discussions involving the implementation and interpretation of the molecular dynamics experiments. We thank Dr. Fred Guengerich for assistance with the stopped-flow experiments and global fitting with KinTek software. We thank Emily Olson Dumas and Daniel Bow for helpful discussions of DDI modeling.

Authorship Contributions

Participated in research design: Glass, Leddy, Orwin, K. Furge, L. Furge

Conducted experiments: Glass, Leddy, Orwin, Miller, K. Furge, L. Furge

Performed data analysis: Glass, Leddy, Orwin, K. Furge, L. Furge

Wrote or contributed to the writing of the manuscript: Glass, Leddy, K. Furge, L. Furge

References

Chico LK, Behanna HA, Hu W, Zhong G, Roy SM, and Watterson DM (2009) Molecular properties and CYP2D6 substrates: central nervous system therapeutics case study and pattern analysis of a substrate database. *Drug Metab Dispos* **37:**2204-2211.

Cojocaru V, Winn PJ, and Wade RC (2007) The ins and outs of cytochrome P450s. *Biochim Biophy Acta* **1770:**390-401.

de Waal PW, Sunden KF, and Furge LL (2014) Molecular dynamics of CYP2D6 polymorphisms in the absence and presence of a mechanism-based inactivator reveals changes in local flexibility and dominant substrate access channels. *PloS One* **9:**e108607.

Dickson BM, de Waal PW, Ramjan ZH, Xu HE, and Rothbart SB (2016) A fast, open source implementation of adaptive biasing potentials uncovers a ligand design strategy for the chromatin regulator BRD4. *J Chem Phys* **145:**154113.

FDA (2015) Press release: FDA approves new drug treatment for nausea and vomiting from chemotherapy.

FDA (2017) In vitro metabolism and transporter-medicated drug-drug interaction studies: guidance for industry.

Gillam EMJ, Baba T, Kim B-R, Ohmoir S, and Guengerich FP (1993) Expression of modified human cytochrome P450 3A4 in Escherichia coli and purification and reconstitution of the enzyme. *Arch Biochem Biophys* **305:**123-131.

Gillam EMJ, Guo Z, Ueng Y-F, Yamazaki H, Cock I, Reilly PEB, Hooper WD, and Guengerich FP (1995) Expression of cytochrome P450 3A5 in Escherichia coli:

effects of 5' modification, purification, spectral characterization, reconstitution conditions, and catalytic activities. *Arch Biochem Biophys* **317:**374-384.

Glass SM, Martell CM, Oswalt AK, Osorio-Vasquez V, Cho C, Hicks MJ, Mills JM, Fujiwara R, Glista MJ, Kamath SS, and Furge LL (2018) CYP2D6 Allelic Variants *34, *17-2, *17-3, and *53 and a Thr309Ala Mutant Display Altered Kinetics and NADPH Coupling in Metabolism of Bufuralol and Dextromethorphan and Altered Susceptibility to Inactivation by SCH 66712. *Drug Metab Dispos* **46:**1106-1117.

Guengerich FP (2015) Human cytochrome P450 enzymes, in: *Cytochrome P450: Structure, Mechanism, and Biochemistry* (Ortiz de Montellano PR ed), pp 523-786, Springer, New York.

Hanna IH, Kim MS, and Guengerich FP (2001) Heterologous expression of cytochrome P450 2D6 mutants, electron transfer, and catalysis of bufuralol hydroxylation: the role of aspartate 301 in structural integrity. *Arch Biochem Biophys* **393:**255-261.

Huey R, Morris GM, Olson AJ, and Goodsell DS (2007) A semiempirical free energy force field with charge-based desolvation. *J Comput Chem* **28:**1145-1152.

Hutzler JM, Walker GS, and Wienkers LC (2003) Inhibition of cytochrome P450 2D6: structure-activity studies using a series of quinidine and quinine analogues. *Chem Res Toxicol* **16:**450-459.

Livezey MR, Briggs ED, Bolles AK, Nagy LD, Fujiwara R, and Furge LL (2014) Metoclopramide is metabolized extensively by CYP2D6 and is a reversible inhibitor, not inactivator, of CYP2D6. *Xenobiotica* **44:**309-319.

Maekawa K, Adachi M, Matsuzawa Y, Zhang Q, Kuroki R, Saito Y, and Shah MB (2017) Structural Basis of Single-Nucleotide Polymorphisms in Cytochrome P450 2C9. *Biochemistry* **56:**5476-5480.

Morris GM, Goodsell DS, Halliday RS, Huey R, Hart WE, Belew RK, and Olson AJ (1998) Automated docking using a Lamarckian genetic algorithm and empirical binding free energy function. *J Comput Chem* **19:**1639-1662.

Nagy LD, Mocny CS, Diffenderfer LE, Hsi DJ, Butler BF, Arthur EJ, Fletke KJ, Palamanda JR, Nomeir AA, and Furge LL (2011) Substituted imidazole of 5-fluoro-2-[4-[(2-phenyl-1H-imidazol-5-yl)methyl]-1-piperazinyl]pyrimidine Inactivates cytochrome P450 2D6 by protein adduction. *Drug Metab Dispos* **39:**974-983.

Olver I (2015) Role of rolapitant in chemotherapy-induced emesis. *Lancet Oncol* **16:**1006-1007.

Poma A, Christensen J, and Pertikis H (2013) Rolapitant and its major metabolite do not affect the pharmacokinetics of midazolam, a sensitive cytochrome P450 3A4 substrate, in: *Support Care Cancer*.

Rowland P, Blaney FE, Smyth MG, Jones JJ, Leydon VR, Oxbrow AK, Lewis CJ, Tennant MG, Modi S, Eggleston DS, Chenery RJ, and Bridges AM (2006) Crystal structure of human cytochrome P450 2D6. *J Biol Chem* **281:**7614-7622.

Sarkar D (2008) *Lattice: Multivariate Data Visualization with R*. Springer, New York.

Shahrokh K, Orendt A, Yost GS, and Cheatham TE, 3rd (2012) Quantum mechanically derived AMBER-compatible heme parameters for various states of the cytochrome P450 catalytic cycle. *J Comput Chem* **33:**119-133.

Siu YA, Hao MH, Dixit V, and Lai WG (2018) Celecoxib is a substrate of CYP2D6: Impact on celecoxib metabolism in individuals with CYP2C9*3 variants. *Drug Metab Pharmacokin* **33:**219-227.

Team RC (2017) R: A language and environment for statistical computing, R Foundation for Statistical Computing, Vienna, Austria.

Tesaro (2015) Varubi prescibing information.

Trott O and Olson AJ (2010) AutoDock Vina: improving the speed and accuracy of docking with a new scoring function, efficient optimization, and multithreading. *J Comput Chem* **31:**455-461.

VandenBrink BM, Foti RS, Rock DA, Wienkers LC, and Wahlstrom JL (2012) Prediction of CYP2D6 drug interactions from in vitro data: evidence for substrate-dependent inhibition. *Drug Metab Dispos* **40:**47-53.

Vanquelef E, Simon S, Marquant G, Garcia E, Klimerak G, Delepine JC, Cieplak P, and Dupradeau FY (2011) R.E.D. Server: a web service for deriving RESP and ESP charges and building force field libraries for new molecules and molecular fragments. *Nucleic Acids Res* **39:**W511-517.

Wang A, Savas U, Hsu MH, Stout CD, and Johnson EF (2012) Crystal structure of human cytochrome P450 2D6 with prinomastat bound. *J Biol Chem* **287:**10834-10843.

Wang A, Stout CD, Zhang Q, and Johnson EF (2015) Contributions of ionic interactions and protein dynamics to cytochrome P450 2D6 (CYP2D6) substrate and inhibitor binding. *J Biol Chem* **290:**5092-5104.

Wang J, Zhang ZY, Powers D, Wang J, Lu S, and Kansra V (2017) Rolapitant absolute bioavailability and PET imaging studies in healthy adult volunteers. *Clin Pharmacol Ther* **102**:332-339.

Wang J, Zhang ZY, Lu S, Powers D, Kansra V, and Wang X (2018) Effects of rolapitant administered orally on the pharmacokinetics of dextromethorphan (CYP2D6), tolbutamide (CYP2C9), omeprazole (CYP2C19), efavirenz (CYP2B6), and repaglinide (CYP2C8) in healthy subjects. [published online ahead of print August 6, 2018] *Support Cancer Care*. doi: 10.1007/s00520-018-4331-x

Yun CH, Kim KH, Calcutt MW, and Guengerich FP (2005) Kinetic analysis of oxidation of coumarins by human cytochrome P450 2A6. *J Biol Chem* **280:**12279-12291.

Zhou SF (2009) Polymorphism of human cytochrome P450 2D6 and its clinical significance: Part I. *Clin Pharmacokinet* **48:**689-723.

Footnotes:

a.

This work was supported by the National Institutes of Health (L.L.F.) [Grant 1R15GM086767-02]; a grant to Kalamazoo College from the Howard Hughes Medical Institute [52006304] through the Precollege and Undergraduate Science Education Program; and the Cook and Varney Funds of Kalamazoo College.

b.

This work was presented in part at the American Society for Biochemistry and Molecular Biology annual meeting, 2017, Chicago, IL, and the Great Lakes Drug Metabolism and Disposition Discussion Group annual meeting, 2018, Indianapolis, IN.

c.

Send reprint requests to: Dr. Laura Lowe Furge, Department of Chemistry, Kalamazoo College, 1200 Academy Street, Kalamazoo, MI 49006. Laura.Furge@kzoo.edu.

d.

DMD Fast Forward. Published on April 5, 2019 as DOI: 10.1124/dmd.118.085928
This article has not been copyedited and formatted. The final version may differ from this version.

Figure Legends

Figure 1. Structure of rolapitant. Rolapitant contains a spirolactam ring structure with three chiral centers and has a molecular weight of 500.2 g/mol. IUPAC Name: (5S,8S)-8-[[(1R)-1-[3,5 bis(trifluoromethyl phenyl]ethoxy]methyl]-8-phenyl-1,7-diazaspiro[4.5]decan-2-one. The arrow indicates the site of hydroxylation by CYP3A4 to form the major metabolite, M19.

Figure 2. Spectral binding titration of rolapitant with CYP2D6 and CYP3A4. (A) Purified CYP2D6 (1 μM) or (B) purified CYP3A4 (2 μM) was split into two cuvettes. A baseline was taken from 350 to 500 nm. Aliquots of rolapitant were added to the sample cuvette and an equal volume of DMSO was added to the reference. Rolapitant exhibited type I spectral binding with CYP2D6 and CYP3A4 suggesting that it is a substrate for both enzymes. (C) Plot of $\Delta A_{430-395}$ (from panel A) versus concentration of rolapitant. The K_s for rolapitant with 2D6 was determined to be 1.2 ± 0.4 μM. (D) Plot of $\Delta A_{430-395}$ (from panel B) versus concentration of rolapitant. The K_s for rolapitant with 3A4 was determined to be 16 ± 2 μM.

Figure 3. Determination of K_d by stopped-flow spectroscopy. Composite absorbance changes from absorbance maxima and minima ($\Delta A_{390-420}$) over time (4 sec) were created for each rolapitant concentration (1, 5, 10, 25, and 50 µM). Only first 2 sec are shown. At least three replicates of each ligand concentration were averaged and plotted over time. Values for k_{on} and k_{off}, 1.12 x 10^6 $M^{-1}s^{-1}$ and 7.04 s^{-1}, respectively, were determined using KinTek Global Kinetic Explorer software. The K_d was determined to be 6.2 μM by the ratio of k_{off} / k_{on}.

Figure 4. Determination of IC_{50} for rolapitant inhibition of CYP2D6. CYP2D6 Supersomes™ (2 pmol) were incubated with dextromethorphan (10 μM) and varying concentrations of rolapitant (0.05-100 μM). Log concentration is plotted against percent activity dextrorphan product formation relative to a 0 μM inhibitor control. The IC_{50} was 24 μM for rolapitant. Each point represents the mean ± standard deviation of an experiment completed in triplicate.

Figure 5. Lineweaver-Burk analysis of the inhibitory effect of rolapitant on CYP2D6. Metabolism of (A) dextromethorphan or (B) bufuralol at four different concentrations (5, 10, 50, and 100 μM) was examined in the presence of 0 (◆), 10 (■), 50 (▲), and 100 μM (●) rolapitant. Each data point represents an average of an experiment completed in quadruplicate. In reactions with dextromethorphan and bufuralol, the K_m increased with increasing concentrations of rolapitant and the v_{max} value was also affected indicating mixed inhibition.

Figure 6. Dixon analysis of rolapitant inhibition of CYP2D6. The concentration of rolapitant was plotted versus the inverse velocity for each line of (A) dextromethorphan or (B) bufuralol at concentrations 5 (●), 10 (▲), 50 (■), and 100 μM (◆) to yield K_i values of 34 μM and 20 μM in assays with dextromethorphan and bufuralol, respectively. Each data point represents an average of an experiment completed in quadruplicate.

Figure 7. **Comparison of the active site starting position to egress position in channel 2c for rolapitant egress.** Frames from molecular dynamics simulation 2 comparing the starting position of rolapitant at the active site of CYP2D6 to the egress position at the

opening of channel 2c. Rolapitant is shown in turquoise. Select amino acids along channel 2c are shown in orange: Phe112 on the helix B'/B-C loop, Glu293 on the *N*-terminal end of helix I, and Lys245 on helix G. (A) Initial position for rolapitant in the active site of CYP2D6 in a ribbon model. (B) Frame where rolapitant egresses from CYP2D6 via channel 2c. (C). Space-filling model of structure in Panel A; rolapitant is only slightly visible in the active site. (D). Space-filling model of structure in Panel B with rolapitant emerged from channel 2c.

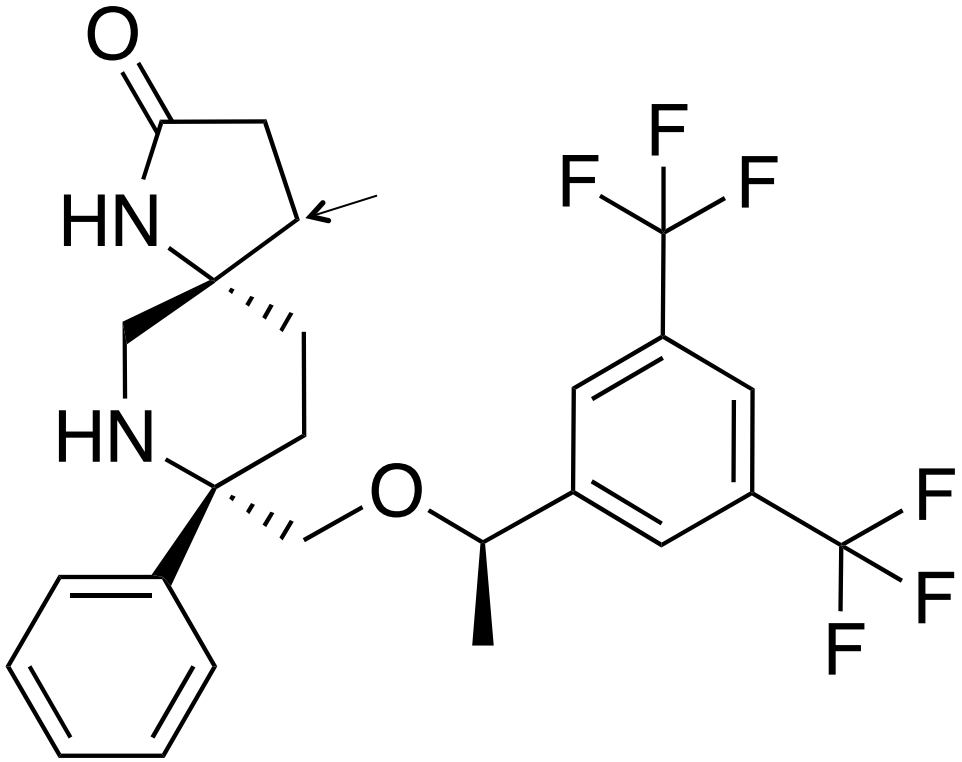

Figure 1

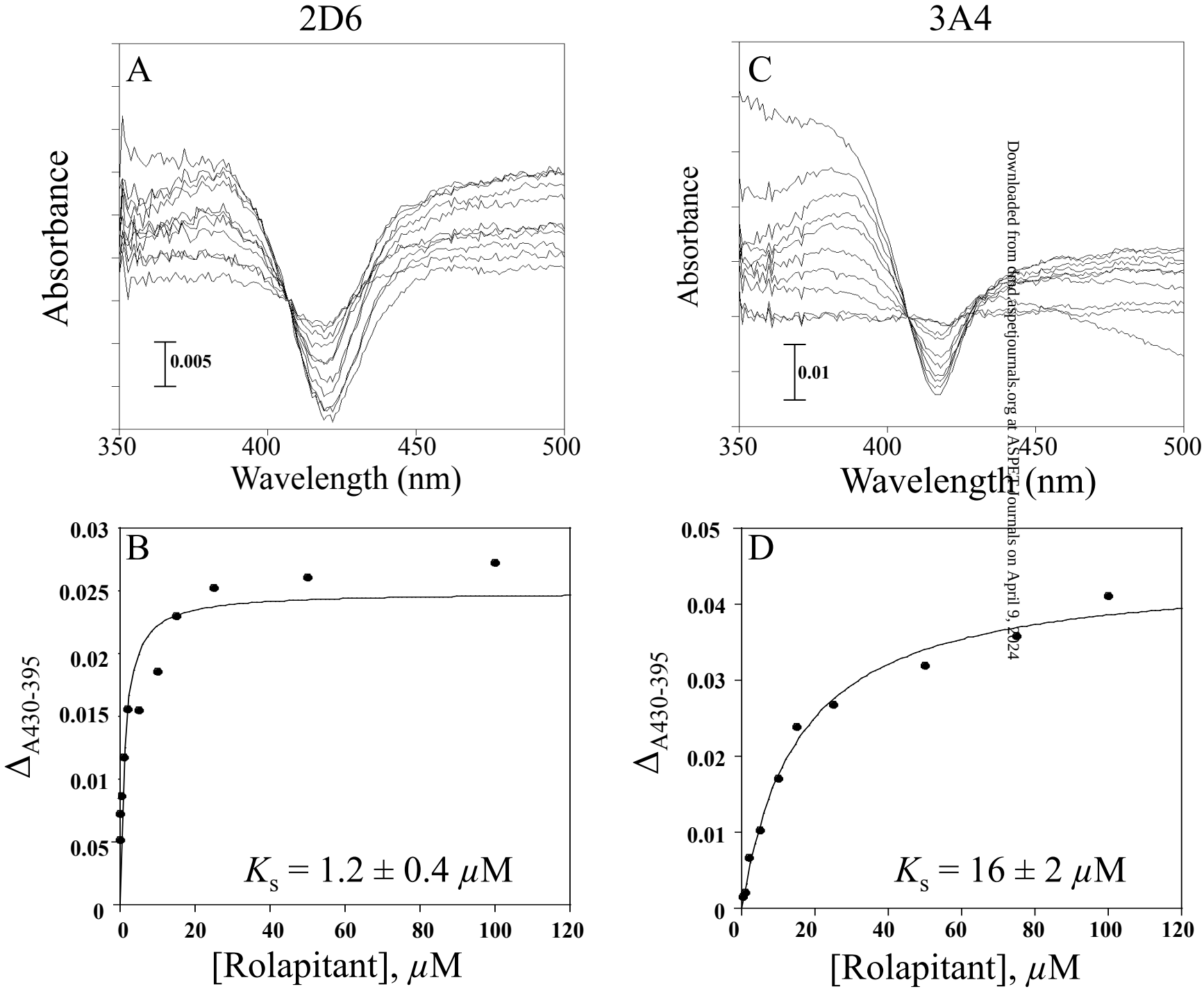

Figure 2

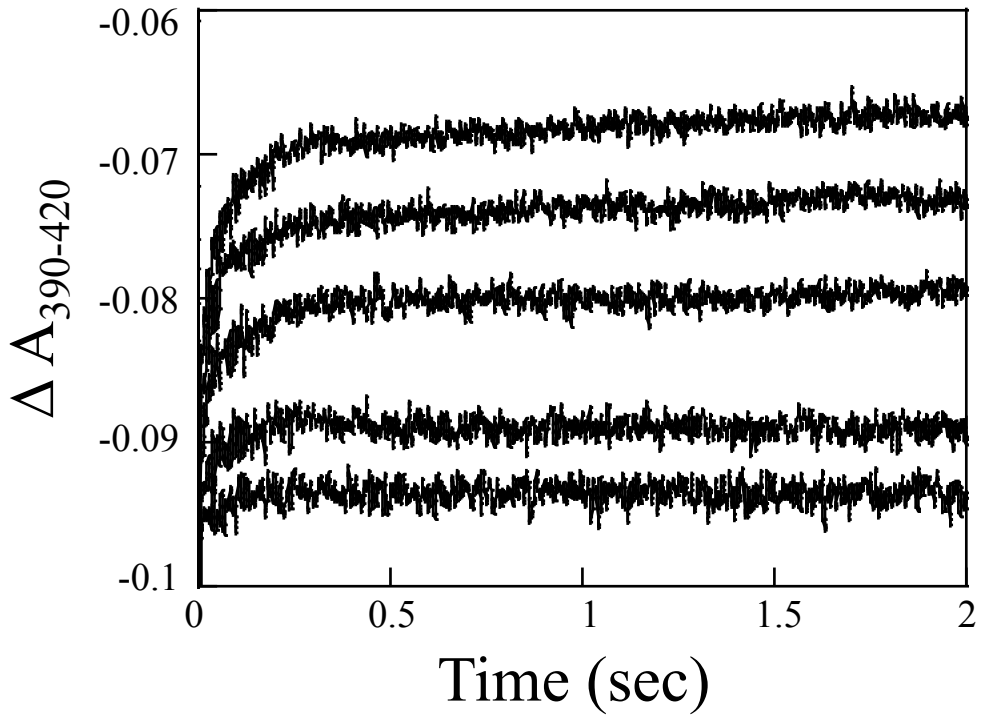

Figure 3

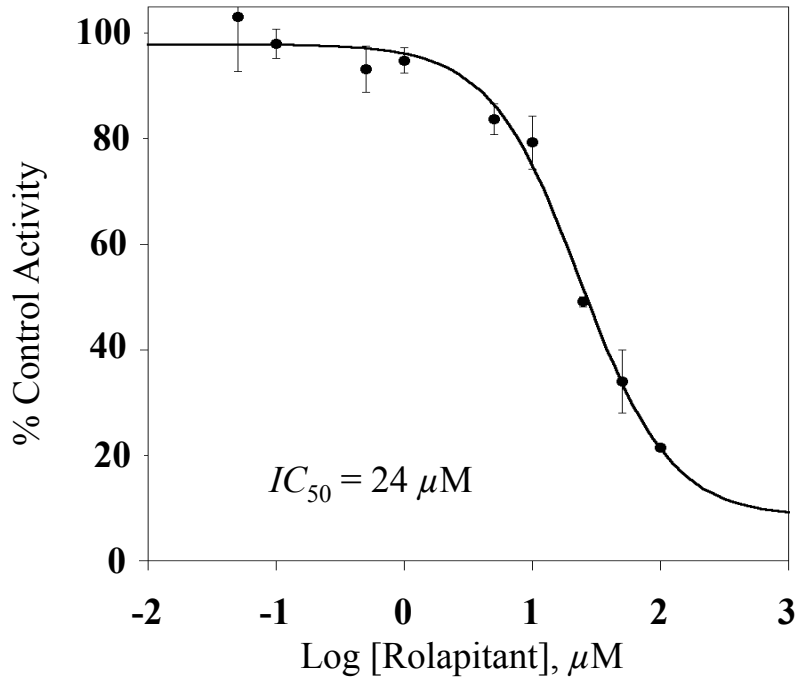

Figure 4

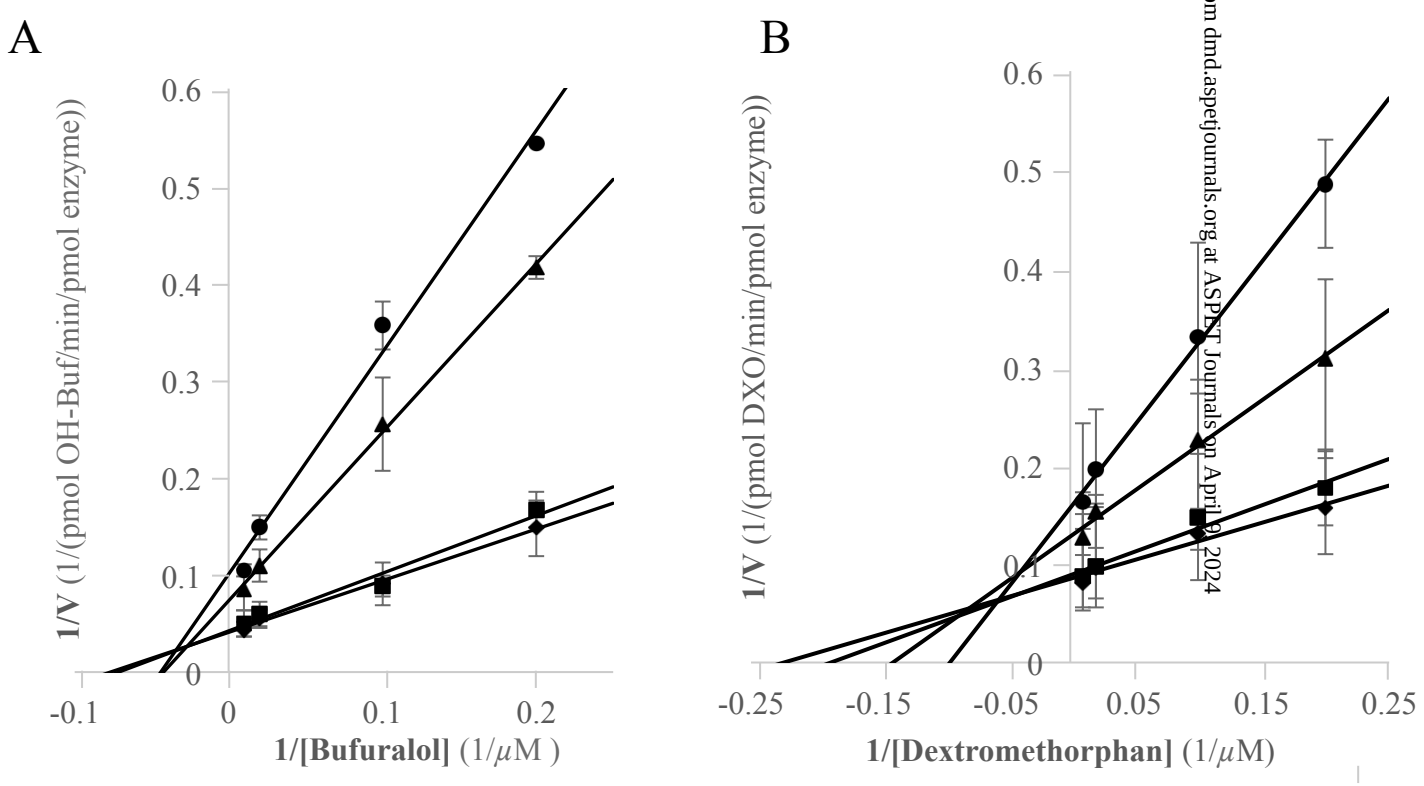

Figure 5

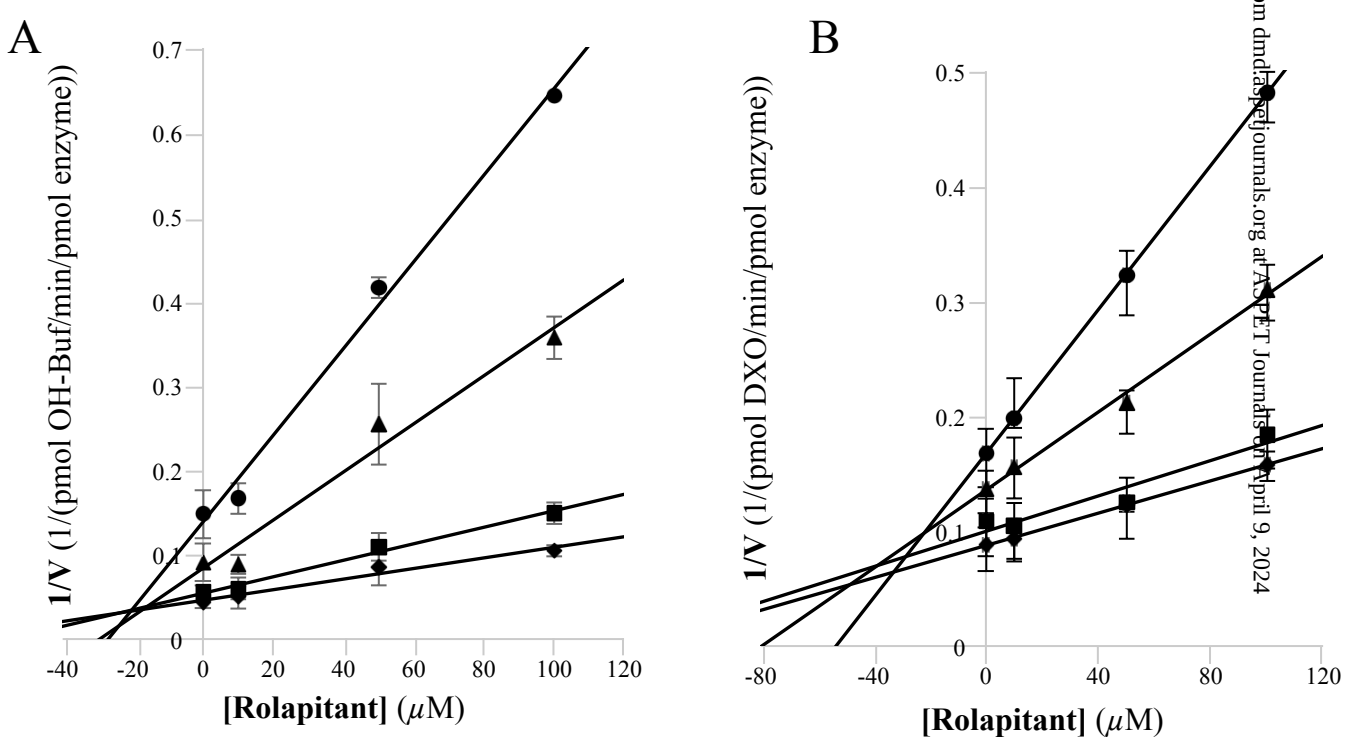

Figure 6

DMD Fast Forward. Published on April 5, 2019 as DOI: 10.1124/dmd.118.085928
This article has not been copyedited and formatted. The final version may differ from this version.

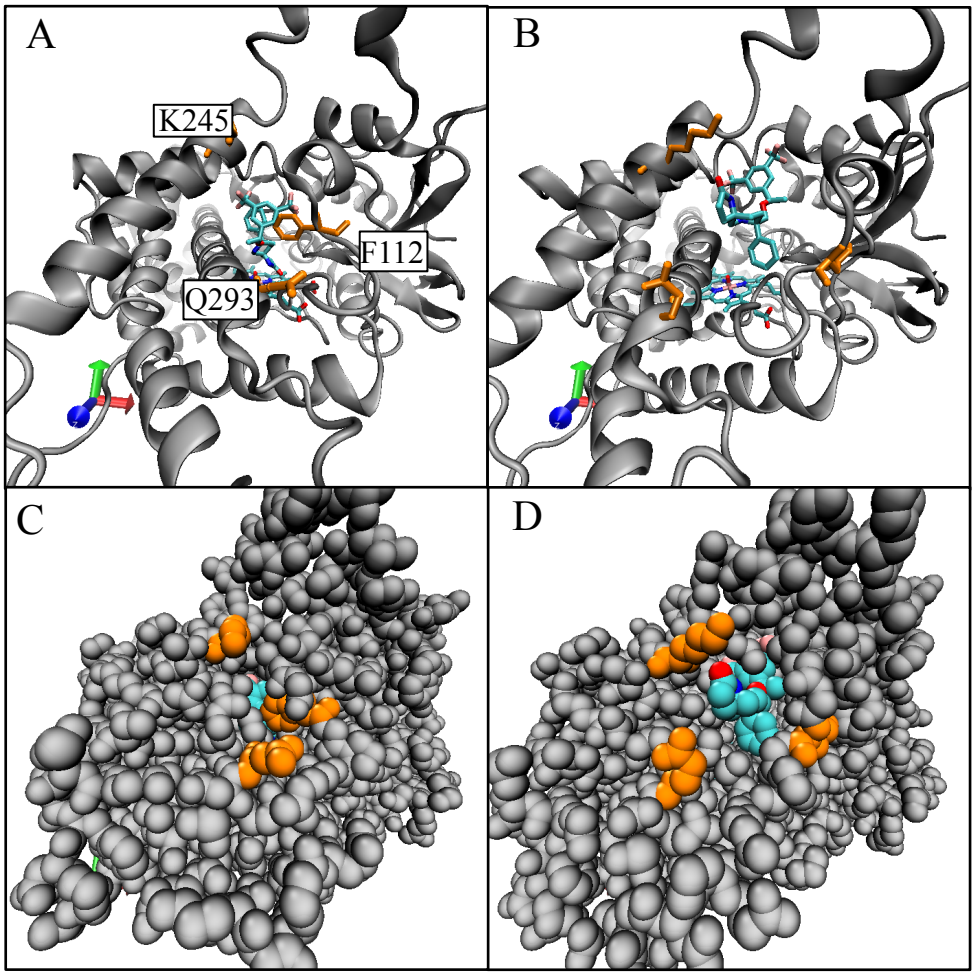

Figure 7

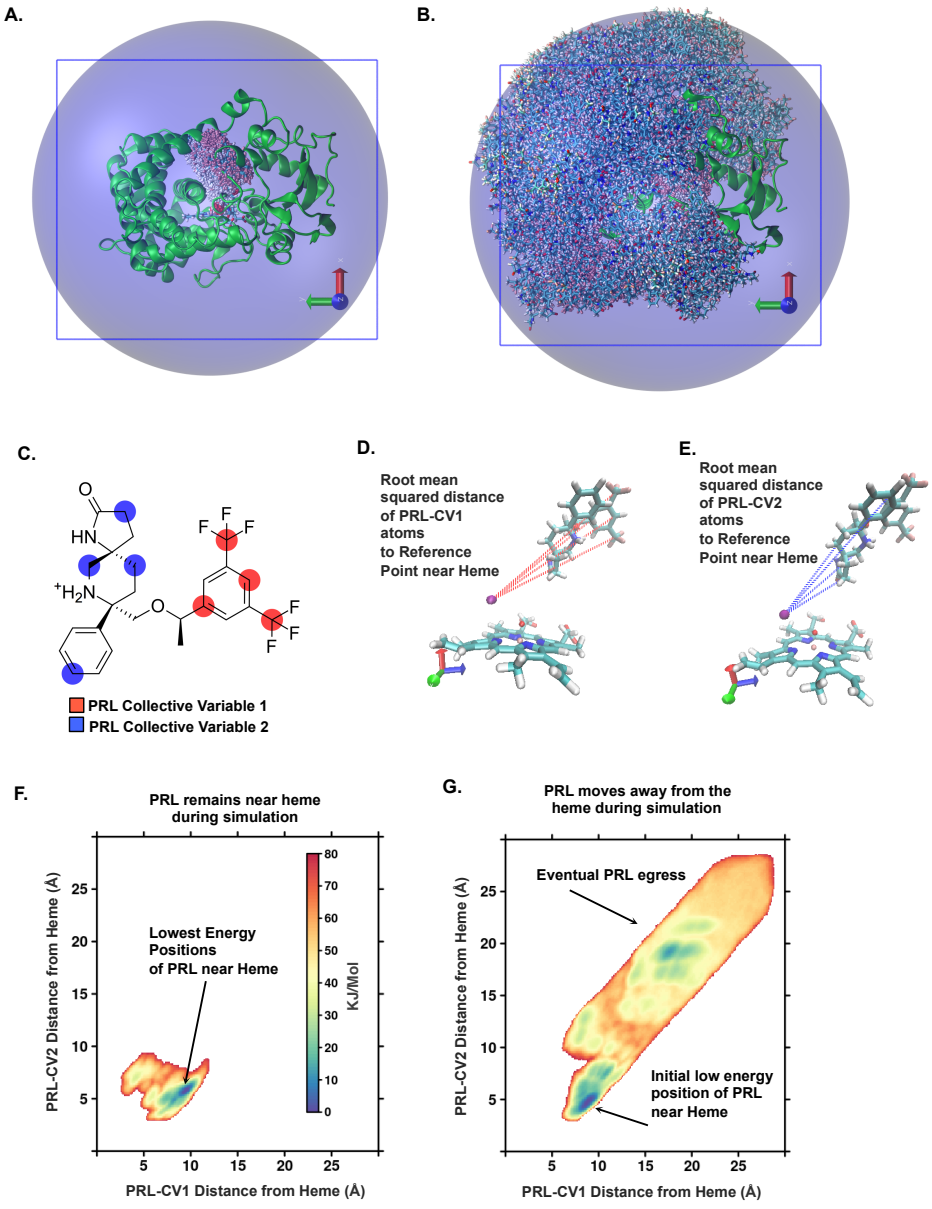

SUPP FIGURE S1. Adaptive Biasing Potential Simulation Configuration. Overview of 1 microsecond simulation of rolapitant /CYP2D6 binding/unbinding. (A, B) CYP2D6 is shown in green and protonated rolapitant (PRL) is shown with CPK colors except for carbon shown in in cyan. The dark blue square represents the periodic box boundary. The light blue sphere represents a spherical restraint to keep rolapitant proximal to the protein. The position of rolapitant is shown every 1 x 10^5 steps of the 5 x 10^8 step simulation. Shown are representative simulations where rolapitant remained in the active site during the entire simulation (A) or exited the active site but did not reenter (B). (C) Atoms of rolapitant that were tracked during the adaptive biasing potential modified simulation. Atoms highlighted in red represent protonated rolapitant-collective variable 1 (PRL-CV1). Atoms highlighted in blue represent protonated rolapitant-collective variable 2 (PRL-CV2). (D, E) Schematic showing root mean squared distance of PRL-CV1 atoms and rolapitant-PRL-CV2 atoms to a reference point near the heme. (F) Example energy landscape of rolapitant that remained in the binding pocket. The lower left corner indicates the PRL-CV1 and PRL-CV2 atoms are closest to the heme. The upper right corner indicates the PRL-CV atom groups are farthest from the heme. The white background indicates space where the CV atoms did not travel. The heatmap shows areas where the CV atoms did travel and positions that were more frequently visited corresponded to lower energy positions. (G) Energy landscape of rolapitant that exited the binding pocket. Note, as the two groups of rolapitant atoms maintain a relatively close proximity to each other throughout the simulation, the energy estimates appear as a diagonal.

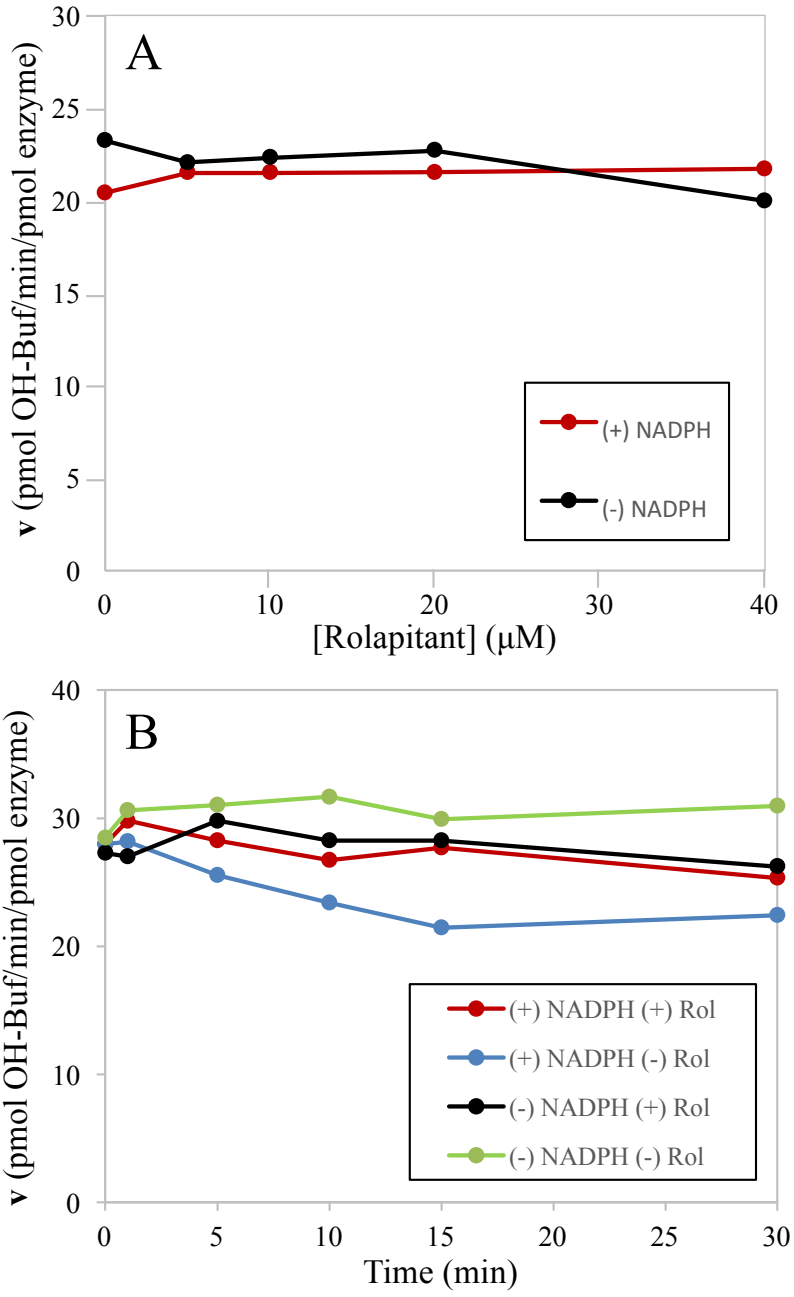

SUPP FIGURE S2: Effect of rolapitant on the activity of CYP2D6 in concentration- and time-dependent inactivation assays. (A) Concentration-dependent inactivation of CYP2D6 by rolapitant (0-40 μM) in 20-minute reactions. (B) Time-dependent inactivation of CYP2D6 by rolapitant (5 μM) for varying time reactions (0 – 30 minutes). Samples were run with and without NADPH and with and without rolapitant as indicated. No concentration- or time-dependent inactivation was observed.

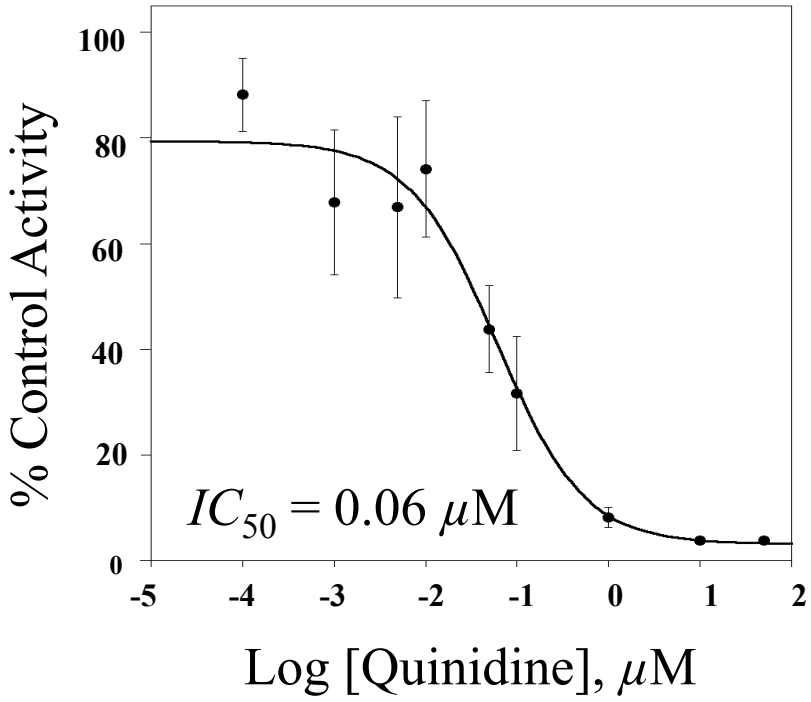

SUPP FIGURE S3. Determination of IC_{50} for quinidine inhibition of CYP2D6. CYP2D6 Supersomes™ (2 pmol) were incubated with dextromethorphan (10 μM) and varying concentrations of quinidine (0 – 50 μM). Log concentration is plotted against percent activity dextrorphan product formation relative to a 0 μM inhibitor control. The IC_{50} was 0.06 μM for quinidine. Each point represents the mean ± standard deviation of an experiment completed in triplicate.

Authors: Glass, Leddy, Orwin, Miller, K. Furge, L. Furge
Title: Rolapitant is a reversible inhibitor of CYP2D6
Journal: Drug Metabolism and Disposition

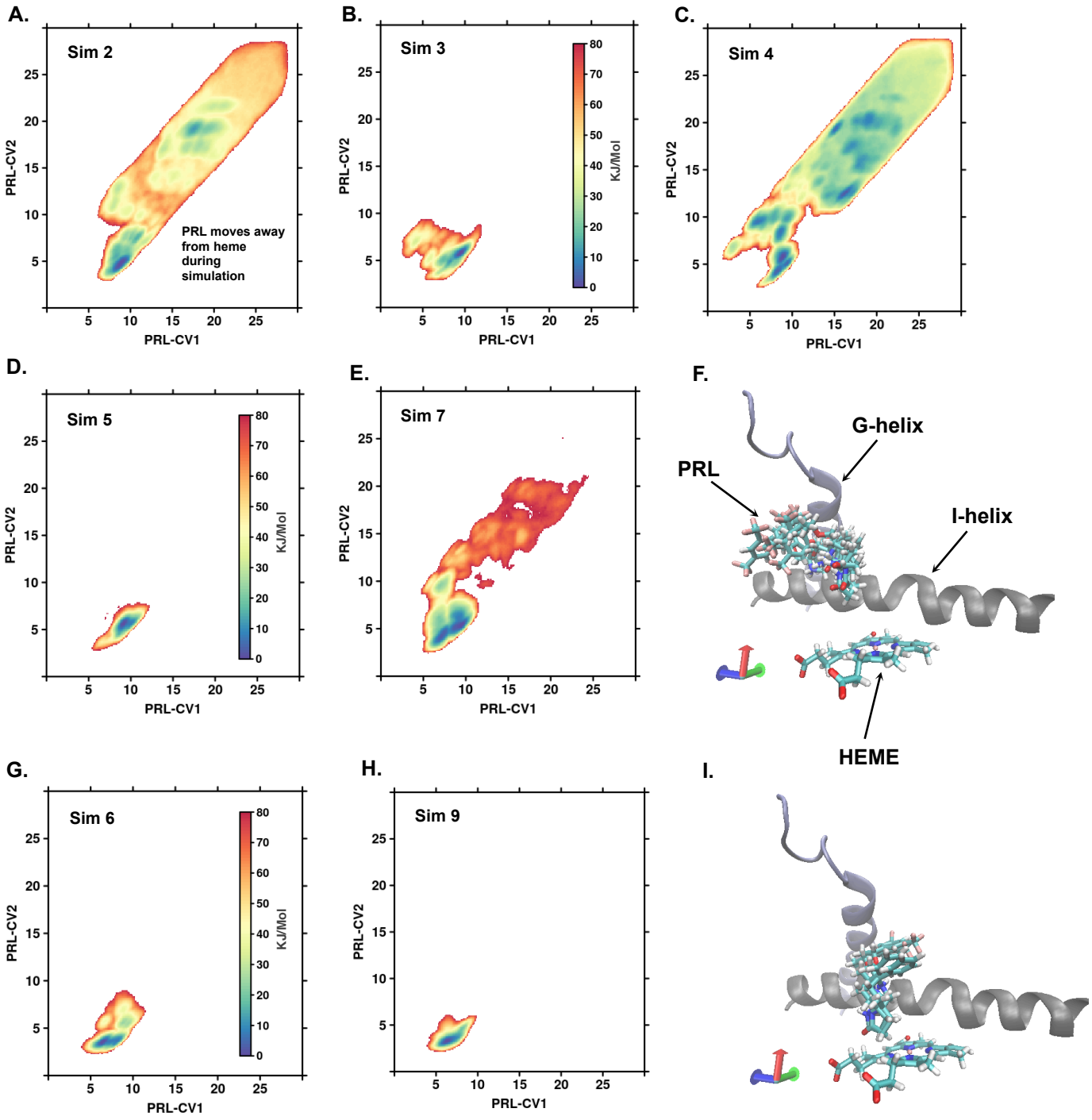

SUPP FIGURE S4 – Part 1 of 2. Energy landscapes and lowest energy binding positions for all simulations. Free energy landscapes are plotted as described in Supp Figure S3. (A-E) Free energy landscapes for simulations 2, 3, 4, 5, and 7 in which protonated rolapitant (PRL) adopted a similar initial low energy pose (shown in panel F)**.** (F) Overlay of rolapitant in the lowest energy pose from simulations 2, 3, 4, 5, and 7. CYP2D6 is shown in grey. The heme and rolapitant are shown with CPK colors. (G,H) Free energy landscapes and (I) overlay of rolapitant low energy poses adopted in simulations 6 and 9. The PRL-CV1 atoms are rotated nearer to the G-helix and rolapitant is closer to the heme as compared to A-E. Free energy landscapes (J,L,N) and rolapitant low energy poses (K,M,O) for simulations 2, 8 and 10. For these simulations rolapitant adopted unique low energy poses.

Authors: Glass, Leddy, Orwin, Miller, K. Furge, L. Furge
Title: Rolapitant is a reversible inhibitor of CYP2D6
Journal: Drug Metabolism and Disposition

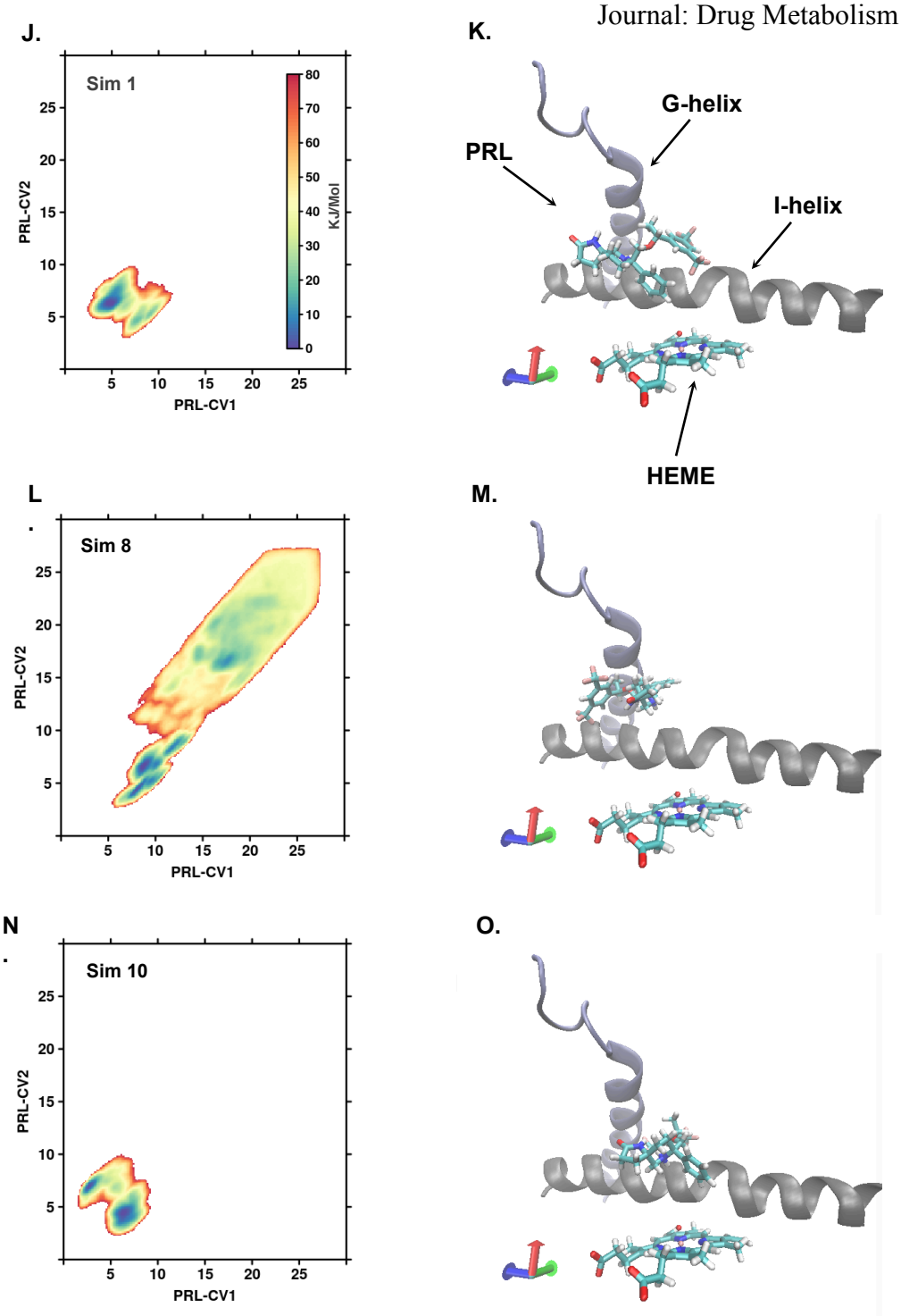

SUPP FIGURE S4 – Part 2 of 2. Energy landscapes and lowest energy binding positions for all simulations. Free energy landscapes are plotted as described in Supp Figure S3. (A-E) Free energy landscapes for simulations 2, 3, 4, 5, and 7 in which protonated rolapitant (PRL) adopted a similar initial low energy pose (shown in panel F)**.** (F) Overlay of rolapitant in the lowest energy pose from simulations 2, 3, 4, 5, and 7. CYP2D6 is shown in grey. The heme and rolapitant are shown with CPK colors. (G,H) Free energy landscapes and (I) overlay of rolapitant low energy poses adopted in simulations 6 and 9. The PRL-CV1 atoms are rotated nearer to the G-helix and rolapitant is closer to the heme as compared to A-E. Free energy landscapes (J,L,N) and rolapitant low energy poses (K,M,O) for simulations 2, 8 and 10. For these simulations rolapitant adopted unique low energy poses.

Authors: Glass, Leddy, Orwin, Miller, K. Furge, L. Furge
Title: Rolapitant is a reversible inhibitor of CYP2D6
Journal: Drug Metabolism and Disposition

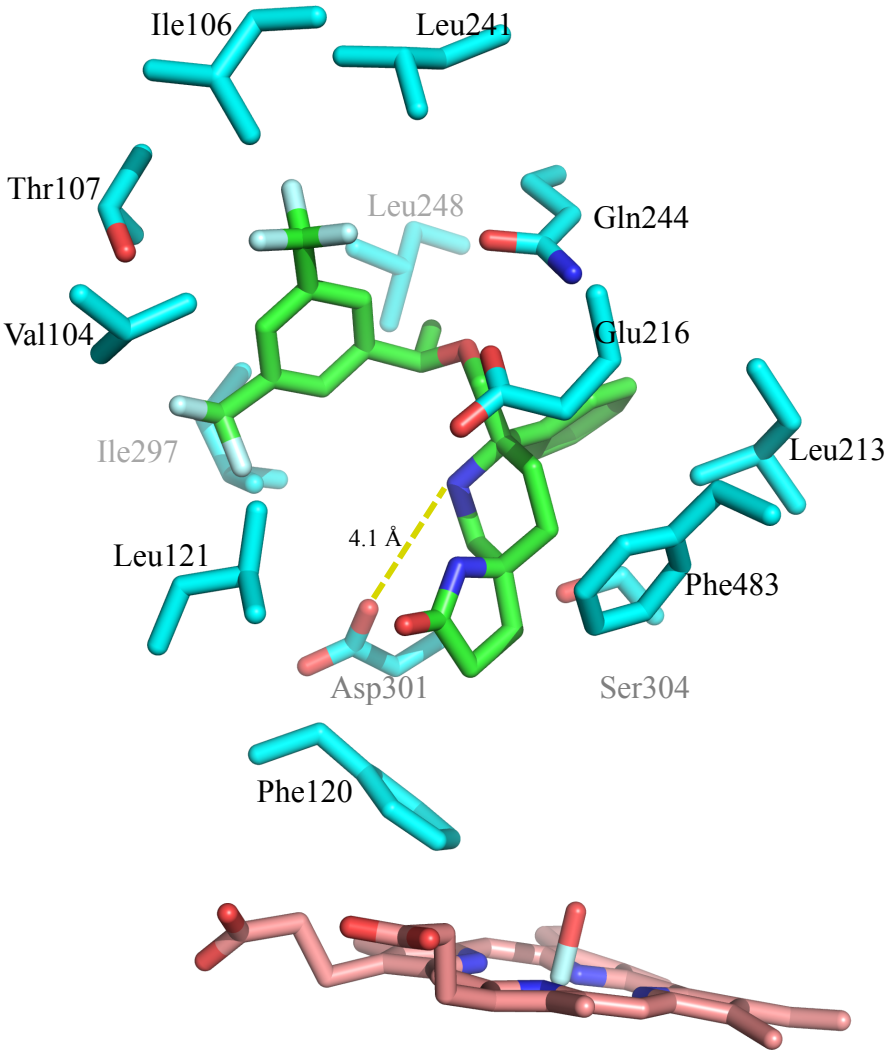

SUPP FIGURE S5. Amino acid side chains within 5 Å of rolapitant in channel 2c binding site. Amino acids side chains (turquoise carbons) within 5 Å of rolapitant (green carbons) are shown along with the heme prosthetic group (pink carbons) as stick figures. The dashed lines identify hydrogen bonds between Asp301 and the protonated nitrogen of rolapitant (4.1 Å). The oxygen ether of rolapitant interacts with Glu216 (4.3 Å) and with Gln244 (3.9 Å) that also interact with each other (3.3 Å). Nitrogen, oxygen, and other heteroatoms (fluorine and iron) are colored dark blue, red, and light blue, respectively. Amino acids are identified by three letter amino acids codes and by residue number.